Bioactive Materials 30 (2023) 116–128

Contents lists available at ScienceDirect

Bioactive Materials

journal homepage: www.keaipublishing.com/en/journals/bioactive-materials

Rational design of oral drugs targeting mucosa delivery with gut organoid platforms

Tianjian Tong [a], Yijun Qi [b], Derrick Rollins [b,e], Luke D. Bussiere [c,d], Debarpan Dhar [c,d], Cathy L. Miller [c,d], Chenxu Yu [a,**], Qun Wang [b,*]

[a] Department of Agricultural Biosystem and Engineering, Iowa State University, Ames, IA, USA
[b] Department of Chemical and Biological Engineering, Iowa State University, Ames, IA, USA
[c] Department of Veterinary Microbiology and Preventive Medicine, College of Veterinary Medicine, Iowa State University, Ames, IA, USA
[d] Interdepartmental Microbiology Program, Iowa State University, Ames, IA, USA
[e] Department of Statistics, Iowa State University, Ames, IA, USA

ARTICLE INFO

Keywords:
Oral drug delivery vehicles
Organoids
Biomimetic virus
Sigma 1 protein
Gold and silica nanoparticles

ABSTRACT

Effective oral drugs and vaccines require high delivery efficiency across the gastrointestinal epithelia and protection of medically effective payloads (i.e., immunogens) against gastric damage. In this study, hollowed nanocarriers (NCs: silica nanospheres and gold nanocages) with poly-l-lysine (PLL) coating and mammalian orthoreovirus cell attachment protein σ1 functionalization (NC-PLL-σ1) were explored as functional oral drug delivery vehicles (ODDVs). The transport of these ODDVs to mucosal lymphoid tissues could be facilitated by microfold cells (M-cells) mediated transcytosis (via σ1-α2–3-linked sialic acids adherence) across gastrointestinal epithelia. PLL coating provided protection and slow-release of rhodamine 6 G (R6G), a model payload. The transport effectiveness of these ODDVs was tested on intestinal organoid monolayers *in vitro*. When compared with other experimental groups, the fully functionalized ODDV system (with PLL-σ1) demonstrated two significant advantages: a significantly higher transport efficiency (198% over blank control at 48 h); and protection of payloads which led to both better transport efficiency and extended-release of payloads (61% over uncoated carriers at 48 h). In addition, it was shown that the M cell presence in intestinal organoid monolayers (modulated by Rank L stimulation) was a determining factor on the transport efficiency of the ODDVs: more M-cells (induced by higher Rank L) in the organoid monolayers led to higher transport efficiency for ODDV-delivered model payload (R6G). The fully functionalized ODDVs showed great potential as effective oral delivery vehicles for drugs and vaccines.

1. Introduction

Oral drug and vaccine delivery, specifically that aiming at the intestinal mucosa layer, is viewed as patient-friendly [1,2] as it generally supports pain-free administration. In addition, oral delivery could also have advantages over intravenous and subcutaneous injections as they can be more cost-efficient and are much easier to administer [1–3]. The orally delivered vaccines are targeted to trigger immunological responses in mucosal-associated lymphoid tissues (MALTs), which promote the production of IgAs. Secretory IgAs (SIgAs) play several critical biological functions: protecting the intestine from pathogenic microorganisms [4], directly neutralizing bacteria and viruses affecting mucosal membranes in the respiratory tract (e.g., sinus and lungs), and digestive tract (e.g., stomach and intestines). SIgAs can interfere with intestinal microbiota by both Fab-dependent and Fab-independent mechanisms, and most importantly, they provide a quick response to foreign antigen uptake [4]. As an aftermath of the global COVID-19 pandemic, the demand for effective oral vaccines, both preventive and therapeutic, is expected to rise, as SIgA immunity could set up a better immune defense for the human body in various scenarios [4].

Developing oral delivery systems faces challenges not existing for injection-based administration pathways. Namely, the medically-

Peer review under responsibility of KeAi Communications Co., Ltd.
* Corresponding author. Department of Chemical and Biological EngineeringIowa State University, 1014 Sweeney Hall, Ames, Iowa, 50011, USA.
** Corresponding author. Department of Agricultural Biosystem and Engineering, Iowa State University, 3344 Elings Hall, Ames, IA, 50011, USA.
E-mail addresses: chenxuyu@iastate.edu (C. Yu), qunwang@iastate.edu (Q. Wang).

https://doi.org/10.1016/j.bioactmat.2023.07.014
Received 20 December 2022; Received in revised form 16 July 2023; Accepted 17 July 2023

effective payloads (e.g., drugs and vaccines) need to survive the harsh gastric environment and be transported across the gastrointestinal (GI) mucosal epithelia effectively [2,3]. Effective delivery vehicles (DVs) hold the key to overcoming both of these challenges; they protect the payloads against gastric degradation, and they could be designed to precisely deliver the payloads to their target areas (for example, mucosal-associated lymphoid tissues (MALT) like Peyer's patches) for release to trigger strong medical responses [2]. In the case of vaccines, adjuvants can be loaded onto the same DVs alongside immunogens to promote more robust immune responses. Effective oral DVs hence are critically crucial for oral drug and vaccine development. Quantitative methods and modeling have been widely used for drug discovery and development to inform more efficient and cost-effective manufacturing programs. Physiologically based pharmacokinetic (PBPK) modeling is one of the critical tools under the overarching umbrella of quantitative models, which describe the absorption, disposition, and toxicity of drug substances in the body quantitatively and mechanistically. Animal models have been widely used in preclinical studies of diseases and drug development. However, the high cost and time-consuming process is the major obstacle to a high throughput strategy for assessing the efficacy of drug candidates. In 2023, FDA no longer requires animal tests before human drug trials [5]. Developing biomimetic PBPK models would provide low-cost alternatives and help bridge the gap between animal models and clinical trials. Organoid-based PBPK models can effectively integrate information about the product characteristics, the individual subject's physiology, and the drug's subsequent systemic disposition without conducting *in vivo* PK studies [6–9].

Previously we reported a strategy to use σ1 protein from mammalian reovirus (MRV) to functionalize gold nanocages into artificial virus-like nanocarriers (AVN) that utilize a σ1:Microfold cells (M cells) transcytosis pathway to improve nanocarrier transport across intestinal cell monolayer that mimics the GI wall [2]. However, three key issues must be addressed before the approach can be tested in clinics. Firstly, the AVNs were not protected, and payloads are susceptible to gastric degradation; secondly, after AVN carried the payload through the GI wall by σ1:M transcytosis, the release of the payload in the mucosal space was completely uncontrolled; and thirdly, it was reasoned that M cells are essential for AVNs to function as effective DVs, but the quantitative correlation between M cells and transport efficiency across the GI wall needed to be established. In this study, we aimed to address the first two issues by utilizing poly-l-lysine (PLL) to form an effective coating that serves as both protection and release-control for the nanocarrier systems, with hollowed silica nanospheres as well as gold nanocages as the ODDVs. Silica (SiO2) abundance makes it much more economically feasible than gold as potential carrier material. PLL is a nontoxic polymer used in this study to create a protective layer surrounding the nanocarriers, which also serves as a diffusion barrier to slow the release of payloads from the nanocarriers. σ1 proteins were then conjugated to the PLL coating for specific M-cell targeting. We aimed to provide a complete strategy to produce fully functional oral drug delivery vehicles (ODDVs) that could offer further enhanced efficacy for the oral delivery of drugs and vaccines.

Our second goal was to check the relationship between M cells and to transport performance of σ1-functionalized ODDV. Lau et al. reported that the level of Rank L used to induce M cell differentiation in small intestinal organoids was directly correlated to the number of M cells presented in the developed organoids [10]. Via control of the organoid engineering process (different Rank L levels at 200 ng/mL, 100 ng/mL, and 0 ng/mL, respectively), organoid monolayers with different M cell presence were created, and their effects on the transport of ODDVs and delivery of the model payload were characterized. σ1 protein was extracted from the type 1 Lang (T1L) serotype of MRV. MRV has a diameter of 85 nm [6]. MRV is a non-enveloped virus that consists of a viral core particle comprised of 5 structural proteins (λ1, λ2, λ3, σ2, and μ2) that enclose the viral genome [11]. Outside the core are the outer capsid proteins (μ1 and σ3) and attachment protein σ1, which play critical roles in virus-cell attachment and entry [11]. Among them, the σ1 protein is instrumental in recognizing and interacting with M cells. M cells are specialized cells in the follicle-associated epithelium (FAE) of Peyer's patches [12,13]. M cells can endocytose foreign antigens in the lumen, then transport them from the apical surface to the basolateral surface (Fig. 1a [2]). For MRV, σ1 adheres to α2–3-linked sialic acids on the apical surface of M cell and facilitates the transcytosis of MRV into MALT to create infection on the basolateral surface of enterocytes [14].

Our previous development of gold nanocage AVN was inspired by MRV transcytosis across M cells, and the σ1 protein was the key to exploring this M cell pathway [2]. Since AVN was successfully created via σ1-functionalized gold nanocages, it was reasonable to believe that σ1-induced functionalities would work on nanocarriers other than gold nanocages, and the σ1:M cell pathway offers a universal oral drug/-vaccine delivery strategy regardless of the types of nanocarriers. It should be noted that surface-functionalization with σ1 proteins is a vital part of our design for the nano delivery system, which means solid nanoparticles that can only carry medically-effective payloads (e.g., vaccines) on the surface (2-D loading) would not be the best choices, as the surface sites occupied by the σ1 proteins could not be used for payload, hence limiting the loading capacity on the nanocarriers. Hence, hollowed nanoparticles with interior space available for payload would be preferred. In this study, we chose hollow silica spheres (HSS) and gold nanocages (GNCs) as our nanocarriers. These particles are easy to produce on a large scale and have inert chemical properties that make them nontoxic for medical applications [15–18]. As these particles have void internal space, loading/unloading medically effective payloads can be readily carried out via a diffusion-driven process. To protect the payloads against the harsh gastric environment, PLL, a widely used non-toxic polymer [19], was used to generate a soft coating to seal the payloads inside the nanocarriers for release control (i.e., extended-release) for the payloads as the nanocarriers reached their destination as a result of slow diffusion of the payloads through the PLL coating relative to naked nanocarriers such as the AVN from our previous report [2].

To validate the effectiveness of the ODDVs as transporters and to evaluate the differences in payload protection and release with and without the PLL coating, we used the intestinal monolayer system [2] as an *in vitro* mimic of the GI epithelia. *Trans*-well plates containing organoid monolayer with M cells, which were cultivated from differentiated small intestinal stem cells, were used, in which the intestinal mucosal layer was modeled on the top inserts. MALT sites were modeled by the bottom compartment, as shown in Fig. 1b. Utilizing this M cell monolayer system; we aimed to compare the performance of both fully functionalized ODDVs (e.g., HSS-PLL-σ1/GNC-PLL-σ1) to blank control (payload alone), carrier control (unfunctionalized HSS/GNC), and uncoated carriers (HSS-σ1/GNC-σ1) to transport model payload (e.g., R6G) across the monolayer via M cell-mediated transcytosis pathway. This system is an excellent simulation to evaluate the potential effectiveness of the ODDVs at transporting payloads such as oral drugs and vaccines to reach MALTs.

2. Results and discussion

2.1. Preparation of GNC/HSS nanocarriers and T1L MRV σ1 proteins

Gold and silica nanoparticles are commonly used in oral drug and vaccine delivery research [15–18,20–24]. Due to the superior loading capacities compared to the 2D structures [2,25], hollowed particles were explored for ODDV development. Gold nanocages (GNC) were synthesized by a galvanic replacement reaction of two stages [24,26]. In stage one, silver nanocubes were synthesized to serve as templates. Then, in stage two, a galvanic replacement reaction was utilized to exchange gold into the sacrificing templates (silver nanocubes). As shown in Fig. 2a, a transmission electron microscopy (TEM) image of an individual representative particle, GNC, thus fabricated, showed an average

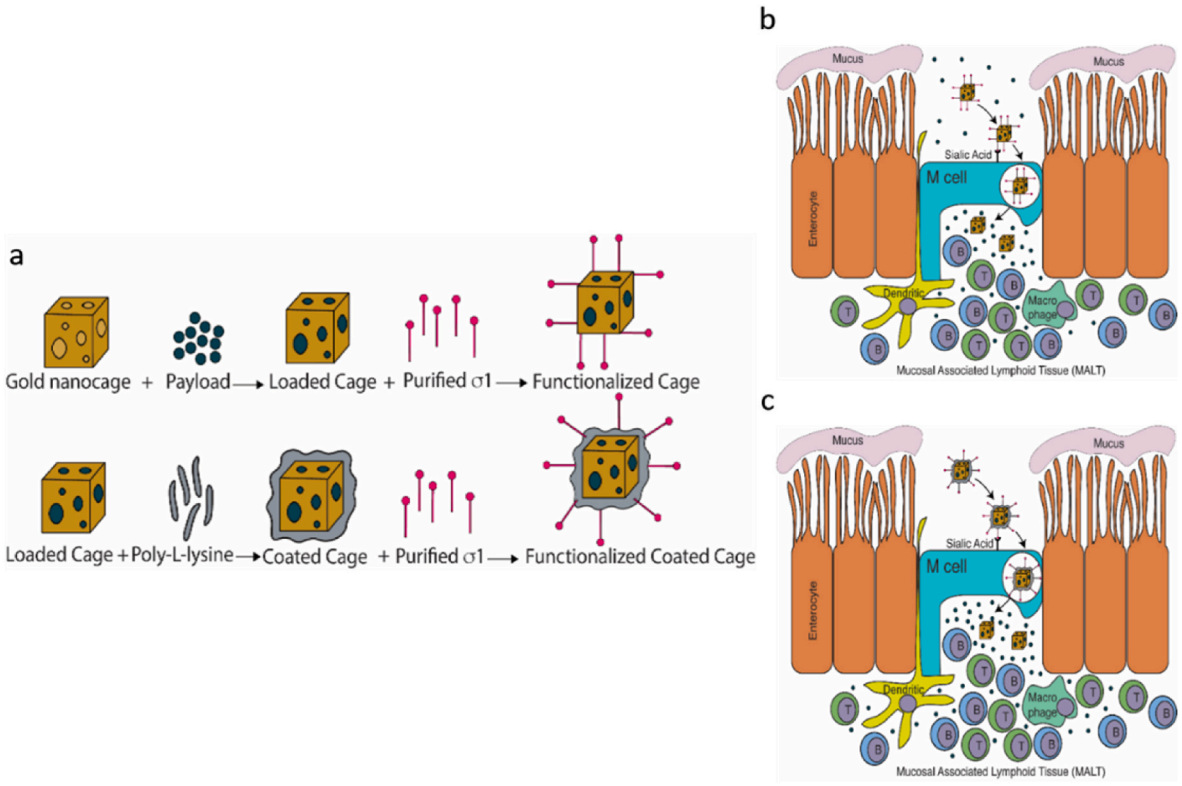

Fig. 1. Scheme: T1L σ1 functionalized ODDVs exploit the M cell transcytosis pathway. (a) Schematic assembly of ODDVs with and without Poly-l-lysine as coating materials, with GNC as the carriers. (b) Schematic of the transport of R6G loaded ODDVs through M cells incorporated into intestinal organoid monolayers. (c) Schematic of the transport of R6G loaded uncoated carriers through M cells incorporated of intestinal organoid monolayers.

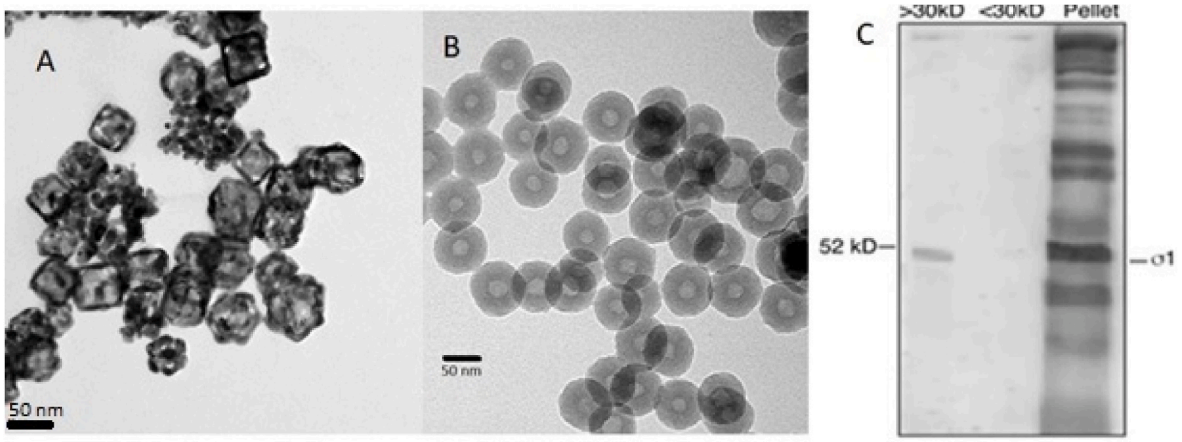

Fig. 2. MRV σ1 functionalization of GNCs and HSSs. (a) TEM image of GNCs showing an average diameter of 40 nm. (b) TEM image of HSSs showing an average diameter of 50 nm. (c) Western blot for pellets after last centrifugation, control group, and T1L σ1 protein (~50 kDa). Following purification, T1L σ1 protein was concentrated by a 30 kDa filter (left lane). Both 30 KDa Filtrated solution (middle lane) and pellets (right lane) served as control groups.

size of 40 nm with pores on the surface, whose size can be controlled via terminating the stage two reaction at specific times. Synthesis of HSS was conducted with reverse microemulsion as templates [25]. Fig. 2b shows the TEM image of a representative individual HSS. The average size of the particles was about 100 nm. A hollowed interior was also observed in the HSS.

T1L MRV σ1 proteins were extracted and purified from MRV as previously described [2,27–29]. The protein preps from MRV were enriched via centrifugation, then filtrated using a 30 kDa cut-off molecular weight filter. The identity of the obtained purified protein samples was confirmed by Western blot using T1L virion anti-sera, which recognizes the σ1 protein [2]. As shown in Fig. 2c, the band at ~50 kDa represents the σ1 protein (left lane). No band was detected in the middle lane of the Western blot, which was the filtrate. These results confirmed that after 30 kDa filtration, there was no unconjugated σ1 protein in the filtrate. In the meantime, the right lane of the Western blot showed all structural proteins from T1L MRV.

The nanocarriers (GNC/HSS) were then coated with PLL via electrostatic physisorption. Then T1L σ1 proteins were conjugated to the nanocarriers via commonly applied NHS-EDC mediated –NH–CO- conjugation chemistry [30] to produce fully-functionalized ODDVs. Uncoated carriers were also produced by directly conjugating T1L σ1 proteins to HSS or GNC nanocarriers without the PLL coating. Model payload (R6G) was uploaded into the interior of the nanocarriers via

diffusion before the coating and σ1 conjugation processes, as described in the materials and methods section.

2.2. Organoid engineering: preparation of M cell incorporated intestinal monolayer

As described elsewhere, 3-dimensional structured small intestinal organoids were derived from mouse small intestinal stem cells [2,30]. Briefly, stem cells were harvested from C3H/HeN mouse small intestine [31]. The growth medium and growth factors (R-spondin 1, Noggin, and EGF), including Matrigel, were added to stem cells [31]. Previous works indicated that Rank L could induce M cell presence in the culture medium of the small intestinal organoids [2,10,32–35]. As shown in Fig. 3B, glycoprotein 2 (GP2) was a marker that confirmed the expression of M cells in the organoids (Fig. 3A) as well as the monolayer samples (Fig. 3C) [2].

In Fig. 3a, we observed the GP2 marker expressed (green) in the Rank L treated organoids but not in the control groups with untreated organoids. These results suggest that only Rank L-treated organoids contained M cells, in agreement with the previous reports [2,10,32–35]. RT-qPCR with GP2-specific primers was utilized to further verify the presence of M cells. The RT-qPCR results (Fig. 3b) confirmed the immunofluorescence results (Fig. 3a) in that only the Rank L-treated organoids showed increased expression of GP2. Again, our work confirmed that adding Rank L into organoids with 3-day incubation induced M cells in the organoids. Once the M cell containing organoids were produced and grown to the proper size (two days after Rank L introduction), their 3-D structure was carefully disrupted, and the cells were re-cultured in *trans*-wells. Rank L has been introduced again into the growth media. After 24 h of incubation, a stable cellular monolayer was formed, miming that of the gastrointestinal epithelia [2,36]. Again, GP2 expressions were only detected in Rank L treated monolayers, as shown in Fig. 3D, and not in the control group, which received no Rank L treatment (Fig. 3C).

2.3. Statistical model

Transport rate (y), in %, continuously increases with time (x), in hours, and thus, a regression modeling approach was used to determine this relationship. The general least squares regression model used in this work is:

$$y_i = f(x_i;\theta) + \varepsilon_i \quad (1)$$

where yi = ith measured response, xi is the ith measured time, θ is a vector of unknown model parameters, $f(x_i;\theta) = \mu_{Y|x_i}$, is the true unknown expectation function (i.e., mean) for yi given xi, and random deviation from that is assumed to be an independent and normally distributed random variable with mean 0 and unknown constant variance, for i = 1, …, n, the sample size, i.e.,

$$\varepsilon_i \overset{indep}{\sim} N(0,\sigma^2) \quad (2)$$

The modeling objective is to estimate the unknown quantities and functions in compliance with the modeling assumptions to make sound formal statistical inferences regarding comparative growth behavior. More specifically, the statistical inference goal is to estimate accurately $\mu_{Y|x_i}$ for a particular case and then statistically assess significant differences using 100(1- a)% confidence intervals (CIs) for and 100(1- a)% individual (i.e., prediction) intervals (PIs) for $y|x_i$ at all experimental values of i, which are called "confidence bands (CBs)" and "prediction bands (PBs)," respectively. The efficacies of the fitted models are supported and evaluated for statistical inference using 95% CBs for $\mu_{Y|x_i}$ and 95% PBs for $y|x_i$.

2.4. Transportation of HSS ODDVs through intestinal monolayers

Transport of both fully-functionalized HSS ODDVs (HSS-PLL-σ1) and uncoated HSS carrier (HSS-σ1) to deliver a small molecule dye (rhodamine 6G, R6G) serving as a model payload was tested with the transwell

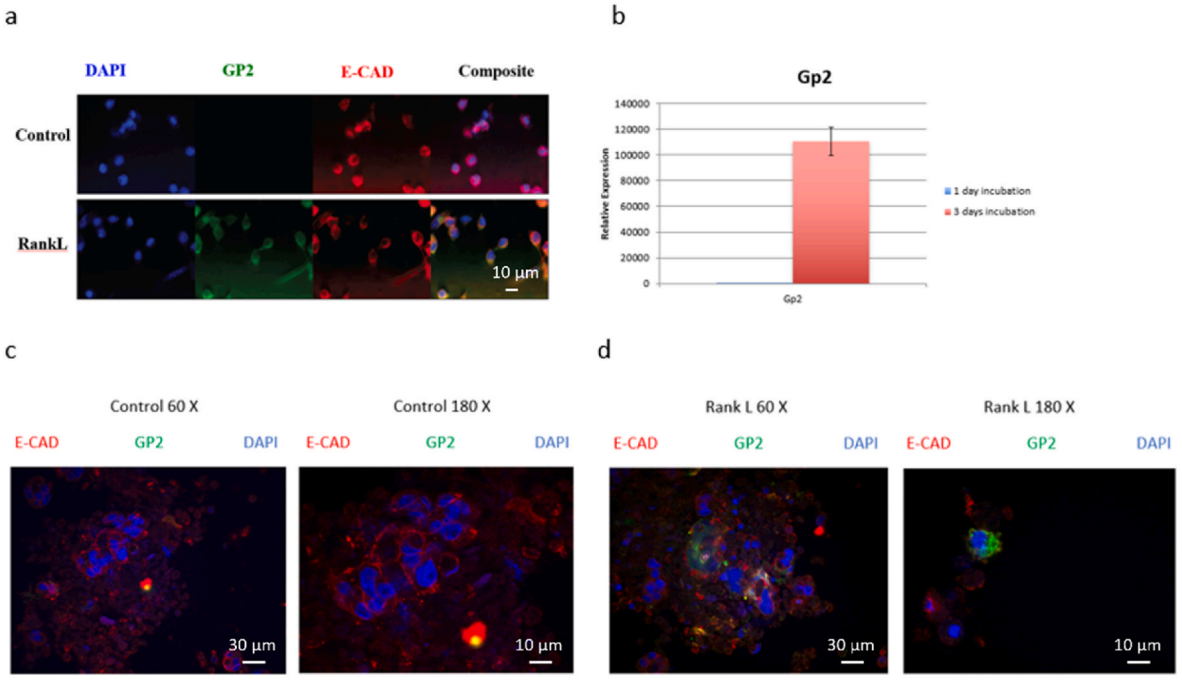

Fig. 3. Detection of microfold cells in 3D mouse organoids and 2D organoid-derived monolayers. (a) Immunofluorescence images of untreated and three-day Rank L-treated 3D organoids stained with antibodies against GP2 (green) and E-Cadherin (red). Nuclei are stained with DAPI (blue). (b) RT-qPCR analysis for expression of GP2-specific mRNA isolated from untreated and Rank L-treated organoids. (c) Immunofluorescence images of untreated organoid monolayers stained with antibodies against GP2 (green) and E-cadherin (red). Nuclei are stained with DAPI (blue). (d) Immunofluorescence images of Rank L-treated organoid monolayers stained with antibodies against GP2 (green) and E-cadherin (red). Nuclei are stained with DAPI (blue). The scale bars in Fig. 3a, c, and 3d are 10 μm and 30 μm, respectively.

organoid monolayer system. As mentioned earlier, the transport of these ODDVs was facilitated by σ1 binding to M cells, which triggers transcytosis through M cells. To confirm that σ1 protein and M cells both were needed for the elevated delivery of the payload across the monolayer to materialize, samples with R6G-loaded HSS nanocarriers without σ1 functionalization were used as HSS carrier control (with M-cell organoids), and small intestinal organoid monolayer without M cells (with ODDVs) was used as monolayer control. The third control, blank control, was set up as a test case in which carrier controls were used in a *trans*-well organoid monolayer system with no M cells; in this case, R6G was transported through the monolayer solely via free diffusion.

The cross-monolayer transport was then monitored by directly measuring the delivery of R6G, a fluorophore that can be readily quantified by measuring the fluorescence intensity across the monolayers. We first compared the performance of uncoated HSS ODDVs concerning the three controls. At time points of 0, 1, 2, 3, 4, 8, 12, 24, 36, and 48 h from the initial addition of HSS-σ1 or HSS into the upper compartment of the transwells, samples were taken from the lower compartments of each of the transwell, and the fluorescence from R6G was measured. The fluorescence intensity data were normalized against the initial R6G fluorescence intensity of the upper compartment at time 0, and the percentage represented the payloads moved across the

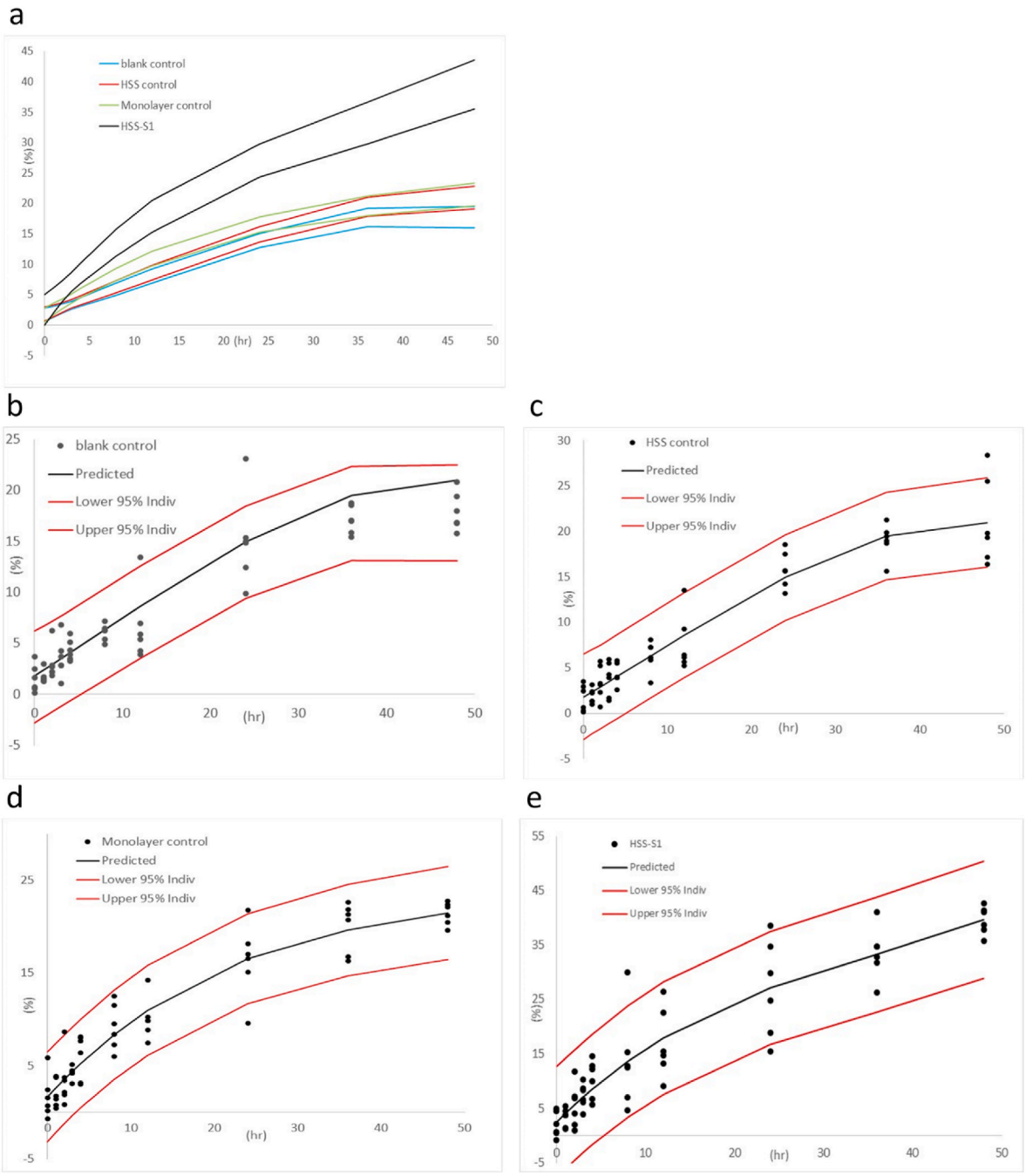

Fig. 4. (a) 95% CBs for Payload (R6G) in different vaccine delivery vehicles (HSS- σ1, HSS) transport across intestinal monolayers, with and without M cell induction over time. (b) Scatter plots for blank control groups change in time. Data represents the estimated mean (central line) and the 95% PBs (upper and lower lines). (c) Scatter plots for HSS control group change in time. Data represents the estimated mean (central line) and the 95% PBs (upper and lower lines). (d) Scatter plots for the Monolayer control group change in time. Data represents the estimated mean (central line) and the 95% PBs (upper and lower lines). (e) Scatter plots for HSS-σ1group change in time. Data represents the estimated mean (central line) and the 95% CBs (upper and lower lines).

monolayers. It should be noted that the baseline (i.e., blank control) represented the free R6Gs released out of the ODDVs in the upper compartment that moved across the monolayers via free diffusion. Our previous report shows no nanocarrier without σ1 functionalization could be transported across the monolayers regardless of M-cell status [2].

Similar patterns as the GNC AVNs reported in our previous work [2] were observed for the HSS ODDVs. As shown in Fig. 4a, transport of R6G by uncoated HSS carriers (with σ1) across the organoid monolayer with M cells was the highest among the four groups. The experimental group HSS ODDV's 95% CBs showed a significant difference from the other three control groups starting at 4 h. No significant difference in transport and payload delivery was observed among the three control groups, as at least one of the two critical conditions (σ1 proteins or M cells) was missing from either of these groups. Thus, it was firmly confirmed that both σ1 and M cells were needed to trigger the movement of the nanocarriers across the monolayer via the M-cell mediated transcytosis pathway. The payload (R6G) effectively delivered by uncoated HSS ODDVs through the M cells was assessed by subtracting the baseline values (i.e., the monolayer control). At 48 h (Fig. 4b), around 18% of the payload (R6G) was delivered by HSS-σ1 nanocarriers into the bottom compartment of our transwell setup, which was slightly less than the

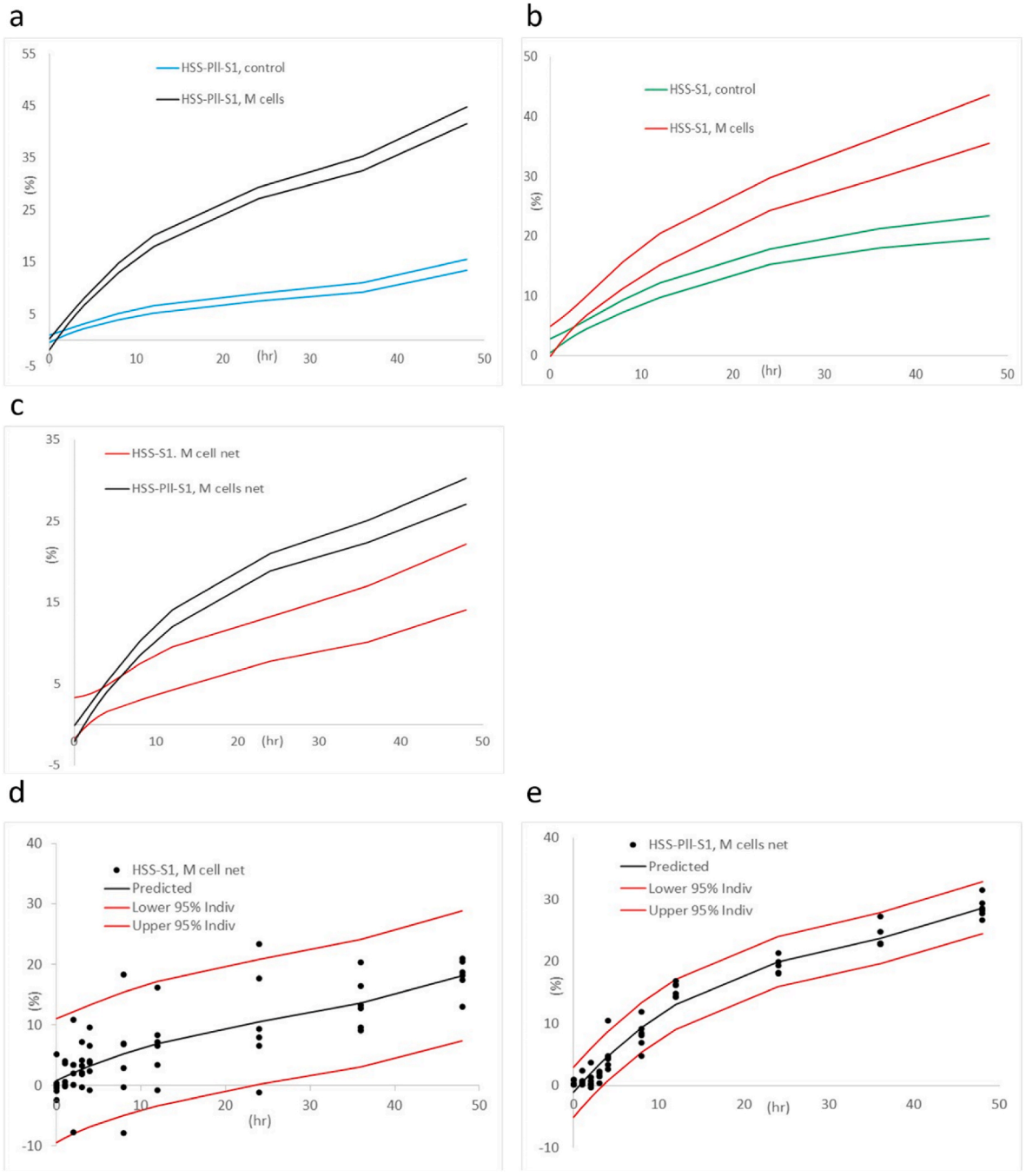

Fig. 5. (a) 95% CBs for Payload (R6G) in HSS- Pll-σ1, transport across intestinal monolayers with and without M cell induction over time. (b) 95% CBs for Payload (R6G) in HSS-σ1, transport across intestinal monolayers with and without M cell induction over time. (c) 95% CBs for net transport by fully functionalized HSS-σ1 ODDV and uncoated HSS-σ1 through intestinal monolayers with M cells incorporated. (d) Scatter plots for change in time for HSS- σ1. Data represents the estimated mean (central line) and the 95% PBs (upper and lower lines). (e) Scatter plots for changes in time for payload transport/release from HSS-σ1 ODDV. Data represents the estimated mean (central line) and the 95% PBs (upper and lower lines).

transport of the payload (R6G) by uncoated GNC AVNs through M cell monolayers (~20%). Given the differences in the shape and size of the nanocarriers, such discrepancies were to be expected. Nonetheless, we can conclude that the ODDVs utilizing the σ1:M cell pathway effectively enhanced the transport/delivery efficiency for payloads, regardless of the materials of the nanocarriers. Fig. 4b shows an estimated time course curve for the payload transport with the blank control group (no ODDVs) and the lower and upper 95% PBs. The data were shown in black dots. Each data set has the same sample number, six in this case. In theory, 95% PBs should contain 95% of the measured values. For the blank control group, 96.7% of the values were with the 95% PBs. Fig. 4c shows the results for the HSS control group (unfunctionalized HSS nanocarriers); 98.3% of the values were within the 95% PBs. Fig. 4d shows the results for the monolayer control group (σ-1 functionalized ODDVs, but no M-cells); 98.3% of the values were within the 95% PBs. And Fig. 4e shows the results for σ-1 functionalized HSS-σ1 ODDV group with M-cells in the monolayer; 95% of the values were within the 95% PBs. These results established that to produce a statistically significant difference in payload transport across the monolayer, fully-functionalized ODDVs and the M-cell in the monolayer are needed. The analyses proved the accuracy and soundness of our approaches.

Next, we tested our hypothesis that the fully functionalized HSS ODDVs (HSS-PLL-σ1) would be more effective in transporting and delivering cargo across the monolayer, with the PLL coating providing protection and release control. Here we compared their transport performance vs. uncoated HSS-σ1 carriers concerning the two monolayer control groups (i.e., with no M-cells). At 0, 1, 2, 3, 4, 8, 12, 24, 36, and 48 h, the transport and delivery of the payloads (R6G) was measured as before. As shown in Fig. 5a, the fully functionalized HSS ODDVs transported more R6G payloads through the M-cell monolayers, showing the σ1:M cell-mediated transcytosis pathway was at work. The 95% CBs of HSS ODDV on monolayers with M cells were significantly higher than that of HSS ODDV on monolayers without M cells from 1 h on. Fig. 5b shows that with M cells present, uncoated HSS-σ1's 95% CBs were also significantly higher than that without M cells. However, the timing of the point of separation was also critical: in the case of fully functionalized HSS ODDV, the point of separation (i.e., the occurrence of the significant difference) was at the 1-h mark, while that of the uncoated HSS-σ1 system did not happen until after 4 h.

It should be noted that consistently higher baseline levels of R6G were observed in the uncoated HSS- σ1/monolayer control group than in the fully functionalized HSS ODDVs/monolayer control group. The baseline level of R6G transport in monolayer control systems (i.e., without M-cells) was determined by free diffusion of released R6G into the top compartment of the transwell across the monolayers. The lower baseline level was caused by less R6G being released from the fully functionalized HSS ODDV system throughout the experiments, which was the direct result of the protection and release control provided by the PLL coating. Furthermore, to better understand the difference between the coated ODDV vs. uncoated. We calculated the net transport of R6G (normalized against monolayer control levels). A different picture emerged. As shown in Figs. 5c and 95% CBs of transport via coated ODDV started to distinguish from that via the uncoated DVs at the 8-h mark. The two groups had no significant differences from 0 to 4 h. From Fig. 5c, we can conclude that from 8 h and on, payloads were diffusing through the PLL coating; this further confirmed the extended release achieved with the functionalized ODDVs.

Fig. 5d and e shows the estimated time course curves of net payload transport and release from uncoated HSS DVs (5 d) and fully functionalized HSS ODDV (5e), with the lower and upper 95% CBs, respectively. The data were shown in black dots. Each data set consists of the same number of samples, six in this case. For the fully-functionalized HSS ODDV set, 98.3% of the values were in the 95% PBs, while the uncoated HSS DV set had 93.3% in the 95% PBs. These results again proved the accuracy and soundness of our approach. These results strongly suggested that PLL coating could slow the diffusion of payload out of the coated nanocarriers, which would protect payloads and could serve as a control mechanism to extend the duration of the payload release at the targeted delivery destination. Thus, we concluded that the PLL coating conjugated with σ1 proteins (defined as "fully functionalized") could provide an effective strategy to optimize 3-D loaded nanocarriers into ODDVs that displayed extended slow release patterns and better delivery efficiency. These characteristics of fully functionalized HSS ODDVs could make them an excellent oral delivery system to transport drugs and immunogens more effectively into the MALTs.

2.5. Transportation of ODDVs through rank L modulated organoids monolayers

It was reasoned that the transport effectiveness of the fully functionalized ODDVs would be directly tied to the presence of M cells in the GI epithelia. To test this hypothesis, both GNC ODDVs and HSS ODDVs with R6G as payload were studied on testbeds (TB0, TB100 and TB200, respectively) of transwell organoid monolayer systems treated with Rank L at three levels (i.e., 0, 100 ng/mL and 200 ng/mL Rank L, respectively). A fourth level (TB400 with 400 μl Rank L) was also investigated. However, at this level, the organoid could not grow normally. Hence it was not pursued further. According to Lau et al., increasing Rank L levels (from 50 ng/mL to 200 ng/mL) increased M-cells in organoid monolayers, evidenced by key M cell markers (e.g., GP2). Hence, the highest Rank L level at 200 ng/mL was expected to induce the highest number of M cells in the testbed TB200, supporting transport (i.e., delivery) of more ODDVs via the σ1-M cell transcytosis pathway. Since the M cell level in animals and humans cannot be manipulated, this organoid engineering approach offered the only way to check the relationship between M cell level and ODDV transport and payload delivery, a unique advantage of such *in vitro* testbeds.

The transport of various ODDVs was monitored by measuring the payload delivery, R6G, across the organoid monolayers. At time points of 0, 1, 2, 3, 4, 8, 12, 24, 36, and 48 h from the initial addition of R6G-loaded ODDVs (e.g., HSS-σ1-PLL, GNC-σ1-PLL, and GNC-σ1) into the top compartment of transwells, samples were taken from the lower compartments of each of the testbeds to quantify the delivered payload R6G via its fluorescence intensity. The fluorescence intensity data were then normalized against each of the total initial R6G fluorescence intensities. The resulting percentage for each case represented how much payload was transported across the organoid monolayers and delivered into the lower compartment.

As shown in Fig. 6a, (e), and (i). GNC + PLL+σ1 ODDV, HSS + PLL+σ1 ODDV, and GNC+σ1 ODDV all show the same pattern of transportation behaviors. In TB0 (0 ng/mL), only low baseline level transport of payload was observed. To be more specific, for all three nanocarriers (fully functionalized ODDVs GNC + PLL+σ1 and HSS + PLL+σ1, and uncoated GNC+σ1), payload transport in TB200 system (i.e., highest M cells) was significantly higher than that of the control (TB0) at 2 h, and that of the TB100 (i.e., lower M cells) at 3 h; while the payload transport in TB100 (low M cells) was significantly higher than that of the control TB0 at 3 h. With 0 ng/mL Rank L, no M cells are expected to be induced in the organoid monolayer. Hence, no σ1-M cell-mediated transcytosis could have occurred in TB0. The payload that crossed over-represented the nano-specific baseline (including the leaking of the R6G from the nanocarriers in the upper compartment and subsequent diffusion through the monolayer, as would be expected for small molecules). The difference between coated (i.e., the –PLL groups) and uncoated ODDVs again indicated the PLL coating's protection effect, which reduced the leakage. In TB100 systems, all three DV groups (HSS-σ1-PLL, GNC- σ1-PLL, and GNC- σ1) showed similar transport performance at ~26%, which increased significantly over that from the control groups (TB0 systems). In TB200 systems, the transport performance was further increased across all groups: HSS-σ1-PLL and GNC-σ1-PLL showed similar transport performance at around 44%, and the GNC-σ1 group was lower at 36.7% (lower due to lack of protection from the

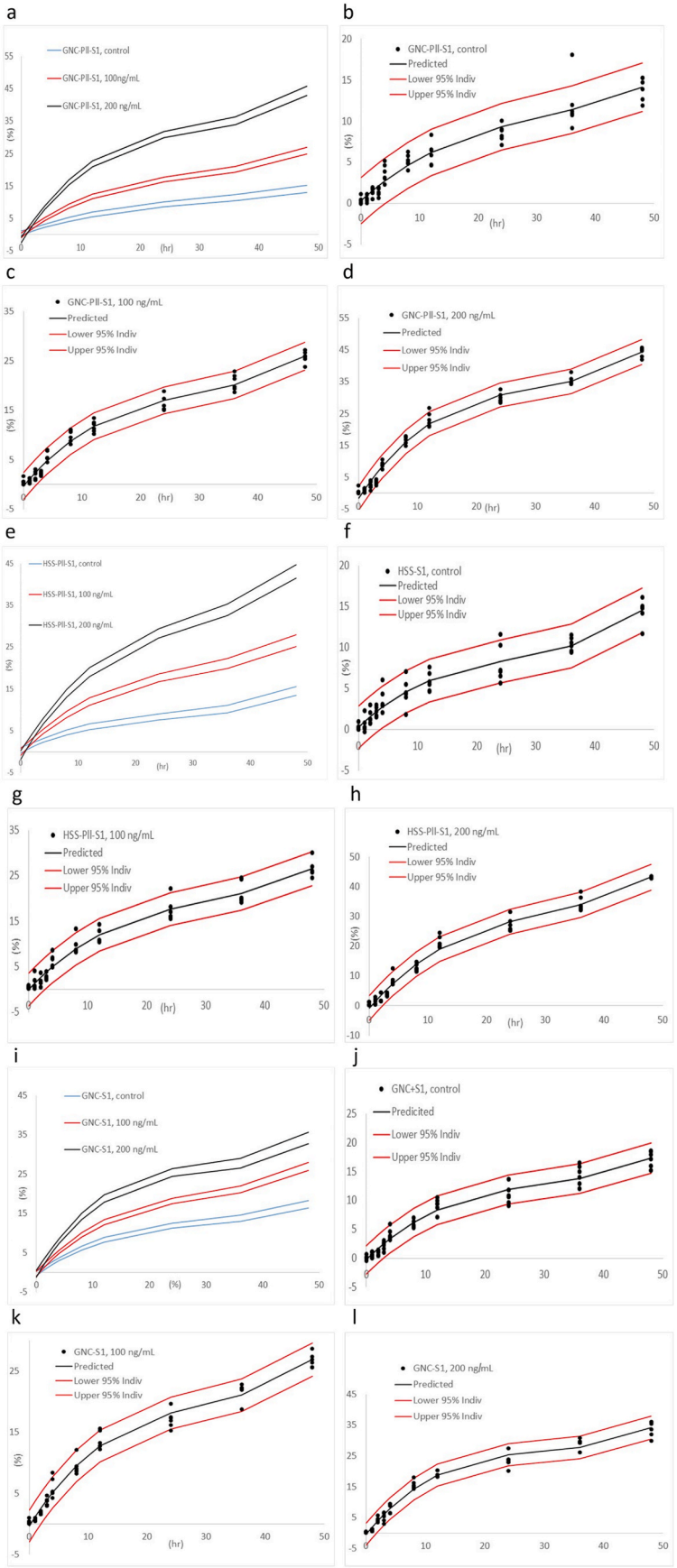

Fig. 6. (a) 95% CBs for Payload (R6G) in GNC-PLL-σ1, transport across intestinal monolayers with different Rank L levels (200 ng/mL, 100 ng/mL, 0 ng/mL). (b) Scatter plots for change in time for GNC-PLL- σ1 on control (0 ng/mL Rank L) monolayers. Data represents the estimated mean (central line) and the 95% PBs (upper and lower lines). (c) Scatter plots for change in time for GNC-PLL- σ1 on 100 ng/mL Rank L monolayers. Data represents the estimated mean (central line) and the 95% PBs (upper and lower lines). (d) Scatter plots for change in time for GNC-PLL- σ1 on 200 ng/mL Rank L monolayers. Data represents the estimated mean (central line) and the 95% PBs (upper and lower lines). (e) 95% CBs for Payload (R6G) in HSS-PLL- σ1, transport across intestinal monolayers with different Rank L levels (200 ng/mL, 100 ng/mL, 0 ng/mL). (f) Scatter plots for change in time for HSS-PLL- σ1 on control (0 ng/mL Rank L) monolayers. Data represents the estimated mean (central line) and the 95% PBs (upper and lower lines). (g) Scatter plots for change in time for HSS-PLL- σ1 on 100 ng/mL Rank L monolayers. Data represents the estimated mean (central line) and the 95% PBs (upper and lower lines). (h) Scatter plots for change in time for HSS-PLL- σ1 on 200 ng/mL Rank L monolayers. Data represents the estimated mean (central line) and the 95% PBs (upper and lower lines). (i) 95% CBs for Payload (R6G) in GNC-σ1, transport across intestinal monolayers with different Rank L levels (200 ng/mL, 100 ng/mL, 0 ng/mL). (j) Scatter plots for change in time for GNC- σ1 on control (0 ng/mL Rank L) monolayers. Data represents the estimated mean (central line) and the 95% PBs (upper and lower lines). (k) Scatter plots for change in time for GNC-σ1 on 100 ng/mL Rank L monolayers. Data represents the estimated mean (central line) and the 95% PBs (upper and lower lines). (l) Scatter plots for change in time for GNC-σ1 on 200 ng/mL Rank L monolayers. Data represents the estimated mean (central line) and the 95% PBs (upper and lower lines).

coating). Fig. 6(b–d) show estimated time course curves for payload transport with GNC + PLL+σ1 ODDV in TB0, TB100 and TB200 testbeds, respectively; Fig. 6(f–h) show estimated time course curves for payload transport with HSS + PLL+σ1 ODDV in TB0, TB100 and TB200 testbeds, respectively; and Fig. 6(f–h) show estimated time course curves for payload transport with GNC+σ1 DV in TB0, TB100 and TB200 testbeds, respectively. All data were black dots with the lower and upper 95% CBs. The number of samples was six in each of these cases. In all cases, more than 95% of data points were within the 95% PBs, confirming our approaches' accuracy and soundness.

In addition, the results were also interesting when we determined the net transport of R6G in testbeds TB100 and TB200 (by subtracting out the baseline transport in TB0). As shown in Fig. 7a and b, in TB100, with or without PLL coating, no significant difference was observed for the GNC ODDVs from 0 to 48 h. This indicated that when the M cell level was relatively low (in TB100), the protection and extended-release control provided by the PLL coating was not the critical contributor to making a significant difference. However, completely different patterns were observed with TB200. We were starting from 8 h on. PLL-coated GNC ODDVs transported and released significantly higher payloads than uncoated GNC ODDVs, and both systems transported significantly higher payloads than those in the TB100 testbeds. These results

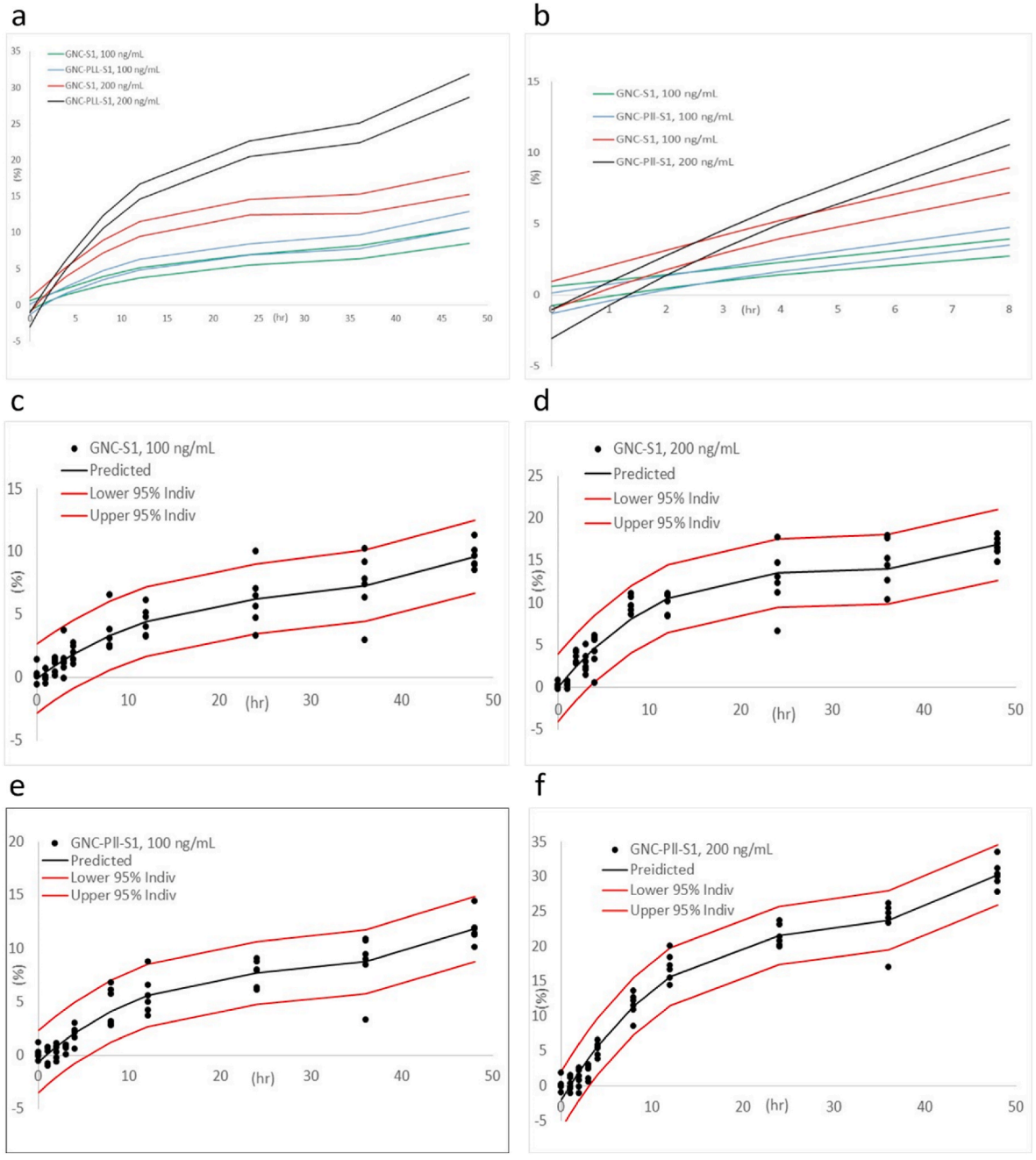

Fig. 7. (a) 95% CBs for net transports of payloads via GNC-ODDVs and GNC-σ1 in testbeds TB200 and TB 100 from 0 to 48 h. (b) 95% CBs for net transports of payloads via GNC-ODDVs and GNC-σ1 in testbeds TB200 and TB 100 from 0 to 8 h. (c) Scatter plots for change in payload transport over time for GNC-σ1 in TB100. Data represents the estimated mean (central line) and the 95% PBs. (d) Scatter plots for change in payload transport over time for GNC-σ1 in TB200. Data represents the estimated mean (central line) and the 95% PBs. (e) Scatter plots for change in payload transport over time for GNC-PLL-σ1 in TB100. Data represents the estimated mean (central line) and the 95% PBs. (f) Scatter plots for change in payload transport over time for GNC-PLL-σ1 in TB200. Data represents the estimated mean (central line) and the 95% PBs.

indicated that at a higher level of Rank L (200 ng/mL), enough M cells were induced in the monolayer testbeds, which caused the higher transport efficiency of the fully functionalized ODDVs to take effects, and the protection and controlled release from the PLL coating became a significant factor as well. It should be noted that though the number of M-cells (represented by the rank L levels in the testbeds) seemed to be the primary driver in determining the payload transport by the ODDVs, the presence of the PLL coating was only secondary. As only in these *in vitro* testbeds can M-cell presence be manipulated via rank L levels, the effects of M cells could only be tested in these systems. As shown in Fig. 7b, the elevated transport with the ODDVs started to go significantly higher at 2 h in TB200 and TB 100 compared to TB0 and 3 h in TB200 compared to TB100. Again, it seems to confirm the critical roles played by the number of M cells in the testbeds; they are the primary drivers for the enhanced transport of payloads by the fully functionalized ODDVs. Fig. 7c–f shows the ranges of CBs and PBs through our data analysis. 95%–98.3% of the measured values were within the 95% CBs and PBs bound. This again proved the accuracy and soundness of our approach, which was consistent throughout our analyses.

Fig. 8a shows that no significant differences were observed between the net payload transport via fully functionalized GNC-ODDV and HSS ODDV (i.e., with PLL coating) across the organoid monolayer testbeds of

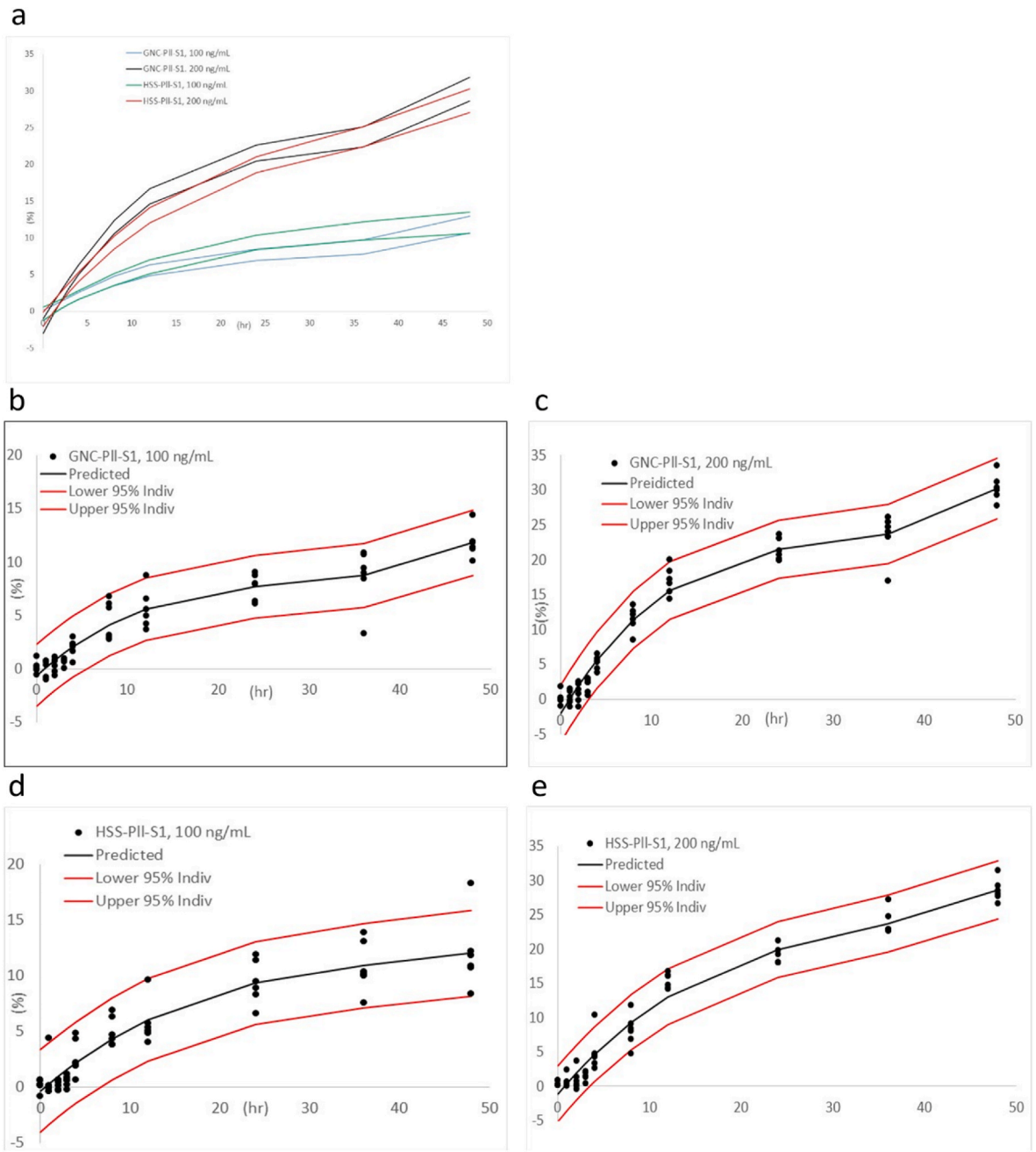

Fig. 8. (a) 95% CBs for net transports of payloads via GNC-PLL-σ1 ODDV and HSS-PLL-σ1 ODDV in testbeds TB200 and TB 100. (b) Scatter plots for change in payload transport over time for GNC-PLL-σ1 in TB100. Data represents the estimated mean (central line) and the 95% PBs (upper and lower lines). (c) Scatter plots for change in payload transport over time for GNC-PLL-σ1 in TB200. Data represents the estimated mean (central line) and the 95% PBs (upper and lower lines). (d) Scatter plots for change in payload transport over time for HSS-PLL-σ1 in TB100. Data represents the estimated mean (central line) and the 95% PBs (upper and lower lines). (e) Scatter plots for change in payload transport over time for HSS-PLL-σ1 in TB200. Data represents the estimated mean (central line) and the 95% PBs (upper and lower lines).

TB100 and TB200, respectively, throughout the 48 h. However, after a short initial stage (~3 h), the net transport of payloads via ODDVs through TB200 started to depart from that through TB100; as time passed, the gap between these two testbeds grew. Specifically, for the GNC-ODDVs, transport in TB200 reached 30% at 48 h, which increased by 154% from that in TB100 (at 11.8%). For the HSS-ODDVs, transport in TB200 reached 28.6% at 48 h, which increased 138% from that in TB100 (at 12%). These results indicated that the M cells themselves were the key to the M cell-mediated transport. Regardless of the materials used to produce nanocarriers, if they were fully functionalized (i.e., with both PLL coating and σ1 conjugation), they gained the capability of utilizing the σ1-M cell-mediated transcytosis pathway to transport payloads across effectively.

Finally, Table 1 shows the R-squared values for the regressional analyses conducted with all the data. In addition to the scatter plots shown in all the figures. We also did residual analyses. As shown, the plots in Figs. 4–8 show a reasonably uniformly random scatter about the mean supporting the assumptions stated by Eq. (2). Hence, the modeling results adequately support the statistical assumptions in Section 2.3.

3. Conclusion

To summarize, firstly, our fully functionalized ODDVs (HSS + PLL+σ1) composed of hollowed silica nanosphere functionalized with MRV receptor binding protein σ1 with Poly-L-Lysine coating were shown to be able to utilize M cell-mediated transcytosis effectively to transport model payloads across an intestinal epithelia mimic (i.e., organoid monolayers), and the PLL coating provided an effective diffusion barrier that could protect the payload, as well as slow down and extend its release. Overall, a much-improved delivery performance (61%) was achieved in the PLL-coated ODDVs vs. uncoated systems. With the σ1:M cell-mediated transcytosis pathway and the PLL payload protection/control release, the HSS + PLL+σ1 ODDVs were highly effective payload delivery vehicles with excellent transporting efficiency. Potentially, they can offer enhanced drug and vaccine delivery across the gastrointestinal mucosa into mucosal-associated lymphoid sites. Secondly, compared to *in vivo* test, the engineered organoid monolayer testbeds had the advantage of manipulating the M cell presence via controlling the Rank L levels. By testing different types of ODDVs (GNC + PLL+σ1 and HSS + PLL+σ1) with these organoid testbeds, it was established that higher M cells in the organoid monolayers resulted from the higher (200 ng/mL) Rank L treatment played primary roles in determining the effectiveness of the transcytosis pathway. The net transport increased by 154% and 138%, respectively, for the two coated ODDVs in the high M-cell TB200 system than in the low M-cell TB100 system.

M cells (controlled via rank L level) were the primary driver for the three critical factors in this nano delivery system. At the same time, PLL coating/σ-1 protein conjugation played secondary yet critical roles in enabling the transcytosis pathway. Types of nanocarriers were a non-factor. Nonetheless, the combination of hollowed 3-D nanocarriers, PLL coating and MRV σ1-protein conjugation offers a complete toolset to produce ODDVs that could be highly effective as oral drug/vaccine delivery vehicles.

Table 1
R-squared values for all experimental groups.

Figure	Experimental group	R^2
4	Black control	0.893
	HSS control	0.909
	Monolayer control	0.906
	HSS-σ1	0.871
5	HSS-σ1 control	0.906
	HSS-σ1 M cell	0.871
	HSS-PLL-σ1 control	0.928
	HSS-PLL-σ1 M cell	0.982
	HSS-σ1 net	0.57
	HSS-PLL-σ1 net	0.966
6	GNC-PLL-σ1 control	0.923
	GNC-PLL-σ1 100 ng/mL	0.978
	GNC-PLL-σ1 200 ng/mL	0.986
	HSS-PLL-σ1 control	0.928
	HSS-PLL-σ1 100 ng/mL	0.964
	HSS-PLL-σ1 200 ng/mL	0.982
	GNC-σ1 control	0.962
	GNC-σ1 100 ng/mL	0.982
	GNC-σ1 200 ng/mL	0.979
7	GNC-PLL-σ1 100 ng/mL net	0.893
	GNC-PLL-σ1 200 ng/mL net	0.968
	GNC-σ1 100 ng/mL net	0.851
	GNC-σ1 200 ng/mL net	0.902
8	GNC-PLL-σ1 100 ng/mL net	0.893
	GNC-PLL-σ1 200 ng/mL net	0.968
	HSS-PLL-σ1 100 ng/mL net	0.864
	HSS-PLL-σ1 200 ng/mL net	0.966

4. Materials and methods

4.1. GNC and HSS fabrication

GNCs Step one: Ethylene glycol (EG) (Sigma-Aldrich) (6 mL) was heated for 1 h in a 160 °C oil bath with stirring. Polyvinylpyrrolidone (PVP) (Sigma-Aldrich) (0.07 g) was added into 3.5 mL EG solution; a mixture was required. AgNO3 (Sigma-Aldrich) (0.12 g) was solved into 2.5 mg EG solution, and a mixture was required. Then 3 mM NaSO4 (Acros) was solved EG solution. Then 70 μl of sodium sulfide solution was added into the ethylene glycol EG solution in the oil bath. After 15 min, 1.5 mL PVP solution and 0.5 mL silver nitrate solution were added. After 10–15 min of reaction, acetone was added to the solution to stop the reaction. Then the solution was centrifuged for 30 min at 1300 rpm. 1 mL of DI water was added to the pellet. Then re-disperse the pellet by sonicating for 1 h. This wash step must be repeated two more times [2].

GNCs step two: 20 mL of DI water is put into a glass vile, and 20 mg of PVP is added to DI water. Then heat and stir the PVP solution to 245 °C and 220 rpm. When the PVP solution was heated to boil, add 200 μL of silver nanocubes made in step one. After 10–15 min, add 2 μL of $HAuCl_4$ (Sigma-Aldrich) every 2 min until the mixture solution turns blue. The wash step is also required. Centrifuge at 2000 g for 30 min at room temperature, then remove the supernatant and add new DI-water. Then re-disperse the pellet by sonicating it for an hour. Then centrifuge at 9000 g for 10 min, remove the supernatant and re-disperse. The last step needs to be repeated once [2].

HSSs: HSSs synthesis consists of two phases mixing at room temperature. The water phase was prepared by mixing 3 μL of (3-aminopropyl) triethoxysilane (APS) (Acros Organics) and 1.1 ML DI-water together. The oil phase was prepared by mixing 4.47 or Triton X-100 (Acros Organics), 3.64g of n-octanol (Fisher) and 14.5 g of cyclohexane (Fisher). Then the water phase was collected and added to the oil phase. After mixing for 30 min, 200 μL of NH_4OH and tetraethylorthosilicate (TEOS) (Acros Organics) were added to water-oil mixing. The reaction was stirred at room temperature for 24 h. Acetone was added to the solution to stop the reaction. Then three times, wash with ethanol and three times with DI water was needed [25].

4.2. T1Lσ1 isolation and purification

L929 mouse fibroblast cells were maintained in Joklik modified minimum essential medium (Sigma-Aldrich) supplemented with 2 mM L-glutamine (Mediatech), 2% bovine calf serum (HyClone), 2% fetal bovine serum, and penicillin (100 IU mL−1)–streptomycin (100 μg mL−1) solution [2]. Type 1 Lang (T1L) MRV was propagated in the L929 cells in the spinner [2]. These cells were then harvested by centrifuged at 3,000g for 10 min. And then, they were resuspended in HO buffer (250 mM NaCl, 10 mM Tris, pH 7.4) and frozen at −80 °C [2, 27]. Then the virus was purified as described in our previous work [2]. After this purification step, digesting with α-chymotrypsin was

necessary to produce infectious subviral particles (ISVPs) [2]. After the purification of ISVPs, we heated ISVPs to 52 °C for 30 min to release σ1 [2]. ISVPs were centrifuged at 35,000 rpm to pellet the ISVPs while σ1 was collected from the supernatant [2,27]. Then σ1 was concentrated by Centricon-30 micro concentration unit (Amicon Crop.) [2,27].

4.3. GNC and HSS functionalization

HSS- σ1 DDV: 2 mL HSS was first incubated with poly-l-lysine (PLL) (w/v 0.1%) and 200 μl R6G. The solution was centrifuged at 9,000g for 10 min, then DI-water was added to re-disperse HSS-PLL. Then (1-ethyl-3-(3-dimethyl aminopropyl) carbodiimide hydrochloride) (EDC) (Thermo Scientific)/N-hydroxysulfosuccinimide (NHS) (Sigma-Aldrich) mix solution was added to HSS-PLL, the solution was incubated for 30 min. The solution was centrifuged at 6,500g for 30 min to remove the excessive EDC/NHS. Then σ1 was added and incubated with HSS-PLL at 4 °C overnight.

HSS- σ1: HSS is the first EDC/NHS procedure to link σ1 protein onto HSS. Then HSS- σ1 was incubated with R6G at 4 °C overnight. Wash with DI water to get rid of excessive R6G.

HSS: incubated with R6G at 4 °C overnight. Wash with DI water to get rid of excessive R6G.

GNC-σ1: GNC was linked to σ1 protein with (1-ethyl-3-(3-dimethylaminopropyl) carbodiimide hydrochloride) (EDC) (Thermo Scientific)/N-hydroxysulfosuccinimide (NHS) (Sigma-Aldrich) procedure. 4- Aminothiophenol was added to the GNC solution and shaken overnight. Then the mix solution was centrifuged for 10 min at 9,000g. After removing the supernatant, Di-water was added to re-disperse the pellet. EDC/NHS solution was added to GNCs and incubated for 30 min at room temperature. Then T1L MRV σ1 protein was added to the GNC solution and incubated at 4 °C overnight. Then the solution was centrifuged at 6,500g for 30 min. Then R6G was added into the GNC-σ1 solution; incubation at 4 °C is required.

GNC-PLL-σ1: poly-l-lysine (PLL) (w/v 0.1%) and 200 μl R6G were added into 2 mL GNC solution, incubated at 4 °C. Then the solution was centrifuged for 10 min at 9000 g. Then we get rid of the supernatant and add DI-water to re-disperse GNC-PLL. Then we use (1-ethyl-3-(3-dimethylaminopropyl) carbodiimide hydrochloride) (EDC) (Thermo Scientific)/N-hydroxysulfosuccinimide (NHS) (Sigma-Aldrich) mix solution to link T1L MRV σ1 protein ono GNC-PLL. After EDC/NHS was added to GNC-PLL, 30 min of incubation were required. And the centrifuge for 30 min at 6,500g. After the excessive EDC/NHS was removed, T1L MRV σ1 proteins were added to GNC-PLL, and incubation must be carried out at 4 °C overnight.

4.4. High-resolution immunofluorescence microscopy

Small intestinal organoids were fixed with 4% paraformaldehyde for 1 h at room temperature. Then were permeabilized for 30 min with 0.5% TritonX buffer (250 μL Triton-X100 in 50 mL PBS). Triple PBS washes were needed. The primary antibody solution was made with 1% PBSA; organoids were stained with the primary antibody at 4 °C overnight. On day 2, secondary antibodies were added to the solution and incubated for 2 h at room temperature. Then triple wash with PBS. 4,6-diamidino-2-phenylindole (DAPI) (EMD Millipore) was used to stain the nuclei of organoids. Fluorescence staining images were acquired by an Olympus®IX81 laser scanning confocal microscope using a 100 × oil-immersion objective. Primary antibody Rat anti-GP2 (MBL International Corporation) was used with a concentration of 2.5 μg mL^{-1}, and secondary antibody goat anti-rat FITC (ThermoFisher) was used at a 1:250 dilution to stain GP2. Primary antibody rabbit anti-E-cadherin (Invitrogen) was used at a 1:250 dilution, followed by a secondary antibody donkey anti-rabbit IgG H&L (Alexa Fluor® 594) (Abcam) at a 1:250 dilution to stain E-cadherin.

4.5. Quantitative RT-qPCR for verifying microfold cell development

Treatment with 1000 μl of Cell recovery solution (Corning Life Sciences) at 4 °C for 1 h of organoids was carried out to remove Matrigel and then washed with PBS twice. RNA extraction was performed using an RNeasy Mini Kit (Qiagen) following the kit's procedure. A Nanodrop spectrophotometer was used to check the concentration and purity of the RNA. For primers, pairs were used. Three of them were purchased from the DNA facility, Iowa State University, Ames, IA: Anxa5 (F: 5′-ATCCTGAACCTGTTGACATCCC-3′; R: 5′-AGTCGTGAGGGCTTCATCATA-3′), GP2 (F: 5′-CTGCTACCTCGAAGGGGACT-3′; R: 5′-CATTGCCAGAGGGAAGAACT-3′) and a primer for the housekeeping gene Gapdh (F: 5′-TTCACCACCATGGAGAAGGC-3′; R: 5′-GGCATGGACTGTGGTCATGA-3′). A Power SYBR™ Green RNA-to-CT™ 1-Step Kit was utilized to complete RT-qPCR.

4.6. Western blot for verifying the presence of σ1 protein

For σ1 protein identification, western blot analysis using rabbit T1L virion antisera at a dilution of 1:1000 was used, followed by a triple-wash with Tris-buffered saline (20 mM Tris, 137 mM NaCl [pH 7.6]) with 0.25% Tween 20 (TBST) buffer. Secondary goat anti-rabbit IgG (BioRad, 170–6518) was used at a dilution of 1:2500, again followed by triple-washes. Lastly, NovaLume Atto Chemiluminescent Substrate AP (Novus Biologicals) was added to the membranes to prepare for imaging on a ChemiDoc XRS Imaging System (Bio-Rad Laboratories) [11].

4.7. Organoid monolayer development

Organoids were cultured for three days using well-established methods [37]. On the 3rd day, 200 ng/mL RankL was added and incubated for another two days to differentiate M cells. Then, 3D structured organoids were disrupted and pipetted into a buffer containing 0.5 mM EDTA. Then the solution was centrifugated at 200g at 4 °C for 5 min. Dissociation of the pellet was achieved by adding 500 μl of 0.05% trypsin/0.5 mM EDTA. Incubation at 37 °C for 4 min was required. 1 mL DMEM/F12 with 10% FBS was added to inactivate the trypsin. The cell suspension went through a 40 μm cell strainer, and then filtered cells were added to solidified 1% Matrigel-coated wells to set up a monolayer. For monolayer setup: on top of the cell layer, 100 μl of culture medium was added; at the bottom and 500 μl of culture medium was added. Monolayers will be ready for experiments after 24 h. For M cell development, 200 ng/mL, 100 ng/mL, and 0 ng/mL RankL were added in the top and bottom compartments.

4.8. Transport of HSS- σ1 ODDV, HSS-σ1, HSS, GNC-σ1 ODDV, GNC-σ1 across intestinal monolayer testbeds

All nanocarriers are loaded with R6G. Initial R6G fluorescence intensities were recorded. 150 μl R6G loaded HSS- σ1 DDV, HSS- σ1, and HSS were added to each transwell. At 0, 1, 2, 3, 4, 8, 12, 24, 36, and 48 h, 50 μl of each sample was collected from the lower compartment of the transwell setup. Then R6G fluorescence intensities were recorded by GLOMAX MULTI DETECTION SYSTEM (Promega) (EX 525, EM 580–640). Each experimental group was conducted in triplicate.

Author contributions

T. T. wrote the paper, fabricated GNCs & HSSs, isolated σ1 protein, assembled GNC- σ1 & HSS- σ1 drug delivery vehicles: σ1 protein and HSS with PLL coating and performed characterization of HSSs, σ1 protein, and HSS- σ1 drug delivery vehicles transport on monolayers. Y. Q. prepared the ISC monolayer system and characterized M cells in 3D and 2D. T. T. and Y. Q. performed imaging, and T.T. and D.R. analyzed data. L.D.B. and D. D. assisted in isolating σ1 protein and imaging. C. L. M., Q. W., and C. Y. provided the laboratory and equipment and edited the

paper. C. Y. and Q. W. provided financial support for the research. C. L. M., Q. W., and C. Y. conceptualized the research, designed the experiment, and supervised the execution of the plan.

Declaration of competing interest

There are no conflicts of interest to declare.

Acknowledgments

Financial support: Dr. Wang is grateful for the support from the National Institute of Biomedical Imaging and Bioengineering (NIBIB) Trailblazer Award (1R21EB032991-01) and the Shanti V. Sitaraman, MD, PhD Inflammatory Bowel Diseases Young Investigator Award (No. 439516). Dr. Yu would like to thank USDA-NIFA (grant no. 2016-07802) and USDA-ARS (award no. 019636–00001) for partially funding this research. The authors thank K. Yoon for assistance in T1L virus purification and qPCR, and B. Bellaire and N. Peroutka-Bigus for assistance in immunofluorescence.

References

[1] N. Lycke, Recent progress in mucosal vaccine development: potential and limitations, Nat. Rev. Immunol. 12 (8) (2012) 592–605.
[2] T. Tong, Y. Qi, L.D. Bussiere, M. Wannemuehler, C.L. Miller, Q. Wang, C. Yu, Transport of artificial virus-like nanocarriers through intestinal monolayers via microfold cells, Nanoscale 12 (30) (2020) 16339–16347.
[3] A.A. Date, J. Hanes, L.M. Ensign, Nanoparticles for oral delivery: design, evaluation and state-of-the-art, J. Contr. Release 240 (2016) 504–526.
[4] N.J. Mantis, N. Rol, B. Corthésy, Secretory IgA's complex roles in immunity and mucosal homeostasis in the gut, Mucosal Immunol. 4 (6) (2011) 603–611.
[5] M. Wadman, FDA no longer needs to require animal tests before human drug trials, Science 379 (2023) 6628.
[6] Z. Zhao, X. Chen, A.M. Dowbaj, A. Sljukic, K. Bratlie, L. Lin, E.L.S. Fong, G. M. Balachander, Z. Chen, A. Soragni, Organoids, Nature Reviews Methods Primers 2 (1) (2022) 94.
[7] Z. Davoudi, N. Peroutka-Bigus, B. Bellaire, A. Jergens, M. Wannemuehler, Q. Wang, Gut organoid as a new platform to study alginate and chitosan mediated PLGA nanoparticles for drug delivery, Mar. Drugs 19 (5) (2021) 282.
[8] H. Peng, N. Poovaiah, M. Forrester, E. Cochran, Q. Wang, Ex vivo culture of primary intestinal stem cells in collagen gels and foams, ACS Biomater. Sci. Eng. 1 (1) (2015) 37–42.
[9] T. Cai, Y. Qi, A. Jergens, M. Wannemuehler, T.A. Barrett, Q. Wang, Effects of six common dietary nutrients on murine intestinal organoid growth, PLoS One 13 (2) (2018), e0191517.
[10] W. de Lau, P. Kujala, K. Schneeberger, S. Middendorp, V.S. Li, N. Barker, A. Martens, F. Hofhuis, R.P. DeKoter, P.J. Peters, Peyer's Patch M Cells Derived from Lgr5+ Stem Cells Require SpiB and Are Induced by RankL in Cultured "Miniguts", Molecular and Cellular Biology, 2012.
[11] L.D. Bussiere, P. Choudhury, B. Bellaire, C.L. Miller, Characterization of a replicating mammalian orthoreovirus with tetracysteine-tagged μNS for live-cell visualization of viral factories, J. Virol. 91 (22) (2017), https://doi.org/10.1128/jvi.01371-17.
[12] J.L. Wolf, R.S. Kauffman, R. Finberg, R. Dambrauskas, B.N. Fields, J.S. Trier, Determinants of reovirus interaction with the intestinal M cells and absorptive cells of murine intestine, Gastroenterology 85 (2) (1983) 291–300.
[13] M. Wang, Z. Gao, Z. Zhang, L. Pan, Y. Zhang, Roles of M cells in infection and mucosal vaccines, Hum. Vaccines Immunother. 10 (12) (2014) 3544–3551.
[14] A. Helander, K.J. Silvey, N.J. Mantis, A.B. Hutchings, K. Chandran, W.T. Lucas, M. L. Nibert, M.R. Neutra, The viral σ1 protein and glycoconjugates containing α2-3-linked sialic acid are involved in type 1 reovirus adherence to M cell apical surfaces, J. Virol. 77 (14) (2003) 7964–7977.
[15] S. Wang, Ordered mesoporous materials for drug delivery, Microporous Mesoporous Mater. 117 (1–2) (2009) 1–9.
[16] M. Sasidharan, H. Zenibana, M. Nandi, A. Bhaumik, K. Nakashima, Synthesis of mesoporous hollow silica nanospheres using polymeric micelles as template and their application as a drug-delivery carrier, Dalton Trans. 42 (37) (2013) 13381–13389.
[17] R.K. Singh, T.-H. Kim, C. Mahapatra, K.D. Patel, H.-W. Kim, Preparation of self-activated fluorescence mesoporous silica hollow nanoellipsoids for theranostics, Langmuir 31 (41) (2015) 11344–11352.
[18] S. Kwon, R.K. Singh, T.-H. Kim, K.D. Patel, J.-J. Kim, W. Chrzanowski, H.-W. Kim, Luminescent mesoporous nanoreservoirs for the effective loading and intracellular delivery of therapeutic drugs, Acta Biomater. 10 (3) (2014) 1431–1442.
[19] M. Stobiecka, M. Hepel, Double-shell gold nanoparticle-based DNA-carriers with poly-L-lysine binding surface, Biomaterials 32 (12) (2011) 3312–3321.
[20] A.E. Gregory, R. Titball, D. Williamson, Vaccine delivery using nanoparticles, Front. Cell. Infect. Microbiol. 3 (2013) 13.
[21] L. Zhao, A. Seth, N. Wibowo, C.-X. Zhao, N. Mitter, C. Yu, A.P. Middelberg, Nanoparticle vaccines, Vaccine 32 (3) (2014) 327–337.
[22] V. Pokharkar, D. Bhumkar, K. Suresh, Y. Shinde, S. Gairola, S. Jadhav, Gold nanoparticles as a potential carrier for transmucosal vaccine delivery, J. Biomed. Nanotechnol. 7 (1) (2011) 57–59.
[23] J.P.M. Almeida, E.R. Figueroa, R.A. Drezek, Gold nanoparticle mediated cancer immunotherapy, Nanomed. Nanotechnol. Biol. Med. 10 (3) (2014) 503–514.
[24] S.E. Skrabalak, J. Chen, Y. Sun, X. Lu, L. Au, C.M. Cobley, Y. Xia, Gold nanocages: synthesis, properties, and applications, Acc. Chem. Res. 41 (12) (2008) 1587–1595.
[25] N. Jatupaiboon, Y. Wang, H. Wu, X. Song, Y. Song, J. Zhang, X. Ma, M. Tan, A facile microemulsion template route for producing hollow silica nanospheres as imaging agents and drug nanocarriers, J. Mater. Chem. B 3 (16) (2015) 3130–3133.
[26] S.E. Skrabalak, L. Au, X. Li, Y. Xia, Facile synthesis of Ag nanocubes and Au nanocages, Nat. Protoc. 2 (9) (2007) 2182–2190.
[27] D.B. Furlong, M. Nibert, B. Fields, Sigma 1 protein of mammalian reoviruses extends from the surfaces of viral particles, J. Virol. 62 (1) (1988) 246–256.
[28] K.A. Dryden, D.L. Farsetta, G. Wang, J.M. Keegan, B.N. Fields, T.S. Baker, M. L. Nibert, Internal/structures containing transcriptase-related proteins in top component particles of mammalian orthoreovirus, Virology 245 (1) (1998) 33–46.
[29] I.I. Mendez, L.L. Hermann, P.R. Hazelton, K.M. Coombs, A comparative analysis of freon substitutes in the purification of reovirus and calicivirus, J. Virol Methods 90 (1) (2000) 59–67.
[30] D. Bartczak, A.G. Kanaras, Preparation of peptide-functionalized gold nanoparticles using one pot EDC/sulfo-NHS coupling, Langmuir 27 (16) (2011) 10119–10123.
[31] A. Fatehullah, S.H. Tan, N. Barker, Organoids as an in vitro model of human development and disease, Nat. Cell Biol. 18 (3) (2016) 246–254.
[32] J.D. Rouch, A. Scott, N.Y. Lei, R.S. Solorzano-Vargas, J. Wang, E.M. Hanson, M. Kobayashi, M. Lewis, M.G. Stelzner, J.C. Dunn, Development of functional microfold (M) cells from intestinal stem cells in primary human enteroids, PLoS One 11 (1) (2016), e0148216.
[33] Y. Yin, D. Zhou, Organoid and enteroid modeling of Salmonella infection, Front. Cell. Infect. Microbiol. 8 (2018) 102.
[34] M.B. Wood, D. Rios, I.R. Williams, TNF-α augments RANKL-dependent intestinal M cell differentiation in enteroid cultures, Am. J. Physiol. Cell Physiol. 311 (3) (2016) C498–C507.
[35] H. Gehart, H. Clevers, Tales from the crypt: new insights into intestinal stem cells, Nat. Rev. Gastroenterol. Hepatol. 16 (1) (2019) 19–34.
[36] G. Altay, E. Larrañaga, S. Tosi, F.M. Barriga, E. Batlle, V. Fernández-Majada, E. Martínez, Self-organized intestinal epithelial monolayers in crypt and villus-like domains show effective barrier function, Sci. Rep. 9 (1) (2019), 10140.
[37] T. Sato, R.G. Vries, H.J. Snippert, M. Van De Wetering, N. Barker, D.E. Stange, J. H. Van Es, A. Abo, P. Kujala, P.J. Peters, Single Lgr5 stem cells build crypt-villus structures in vitro without a mesenchymal niche, Nature 459 (7244) (2009) 262–265.